Int. J. Electrochem. Sci., 6 **(2011)** 5676 - 5688

International Journal of
ELECTROCHEMICAL
SCIENCE
www.electrochemsci.org

Inhibitive Effect of Cefuroxime on the Corrosion of Mild Steel in Hydrochloric Acid Solution

Ashish K. Singh[1, 2,*], *M. A. Quraishi*[2], *Eno E. Ebenso*[1]

[1] Department of Chemistry, School of Mathematical and Physical Sciences,
North-West University (Mafikeng Campus), Private Bag X2046, Mmabatho 2735, South Africa
[2] Department of Applied Chemistry, Institute of Technology, Banaras Hindu University, Varanasi 221005, India
[*]E-mail: singhapc@gmail.com

Received: 11 September 2011 / *Accepted:* 24 October 2011 / *Published:* 1 November 2011

The corrosion inhibition properties of cefuroxime (CFM) for mild steel corrosion in HCl solution was investigated using electrochemical impedance spectroscopy (EIS), potentiodynamic polarization and gravimetric methods. Mixed mode of adsorption (physisorption and chemisorption) is proposed for the inhibition and the process followed the Langmuir adsorption isotherm. The mechanism of adsorption inhibition and type of adsorption isotherm were proposed from the trend of inhibition efficiency with temperature, E_a and ΔG^o_{ads}. Potentiodynamic polarization study clearly revealed that CFM acted as mixed type inhibitor but predominantly cathodic. The experimental data showed a frequency distribution and therefore a modelling element with frequency dispersion behaviour and a constant phase element (CPE) have been used.

Keywords: Adsorption; Corrosion; EIS; Kinetic parameters; Mild steel

1. INTRODUCTION

The damage by corrosion generates not only high cost for inspection, repairing and replacement, but in addition these constitute public risk, thus the necessity of developing novel substances that behave like corrosion inhibitors especially in acid media[1].There always exists a need for developing new corrosion inhibitors. Acid solutions are widely used in industry for acid pickling of iron and steel, chemical cleaning and processing, ore production and oil well acidification. The use of hydrochloric acid in pickling of metals, acidization of oil wells and in cleaning of scales is more economical, efficient and trouble-free, compared to other mineral acids [2]

The corrosion inhibition efficiency of organic compounds is related to their adsorption properties. Studies reported that the adsorption of organic inhibitors mainly depends on some physiochemical properties of the molecule, related to its functional groups, to the possible steric effects and electronic density of donor atoms. Adsorption also depends on the possible interaction of π-orbital of the inhibitor with d-orbital of the surface atoms, which induces greater adsorption of the inhibitor molecules on the surface of mild steel [3-6].

Though the existing data show that numerous N-heterocyclic organic compounds have good anticorrosive activity, some of them are highly toxic to both human beings and environment. The safety and environmental issues of corrosion inhibitors arisen in industries has always been a global concern. Due to increasing environmental awareness and adverse effect of some chemicals, research activities in recent times are geared towards developing cheap, non-toxic and environmentally safe corrosion inhibitors [7-10].

The present article is devoted to study cefuroxime (CFM) as corrosion inhibitor for mild steel in hydrochloric acid solution using electrochemical impedance spectroscopy (EIS), potentiodynamic polarization and weight loss techniques.

Cefuroxime is the commercial name for (6R,7R) 3[(aminocarbonyl)oxy]methyl}-7-[(2E)-2-(2-furyl)-2(methoxyimino)acetyl]amino}-8-oxo-5-thia-1 azabicyclo[4.2.0]oct-2-ene-2-carboxylic acid. The molecular structure of cefuroxime (CFM) is shown in Fig.1. It is a second-generation cephalosporin antibiotic and does not contain any toxic metallic elements.

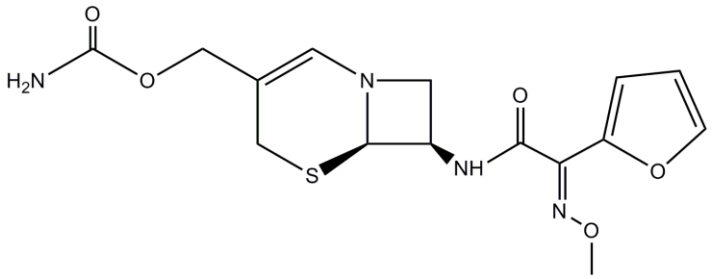

Figure 1. Molecular structure of Cefuroxime (CFM) molecule

2. EXPERIMENTAL

2.1 Inhibitor

Stock solution of CFM was made in 10:1 ratio water: ethanol mixture to ensure solubility. This stock solution was used for all experimental purposes.

2.2 Corrosion measurements

Prior to all measurements, the mild steel specimens, having composition (wt %) C = 0.17, Mn= 0.46, Si = 0.26, S = 0.017, P = 0.019 and balance Fe, were abraded successively with emery papers

from 600 to 1200 grade. The specimen were washed thoroughly with double distilled water, degreased with acetone and finally dried in hot air blower. After drying, the specimen were placed in desiccator and then used for experiment.

The aggressive solution of 1 M HCl was prepared by dilution of analytical grade HCl (37%) with double distilled water and all experiments were carried out in unstirred solutions. The rectangular specimens with dimension 2.5 × 2.0 × 0.025 cm were used in weight loss experiments and of size 1.0 × 1.0 cm (exposed) with a 7.5 cm long stem (isolated with commercially available lacquer) were used for electrochemical measurements.

2.3 Electrochemical impedance spectroscopy

The EIS tests were performed at 303 ±1 K in a three electrode assembly. A saturated calomel electrode was used as the reference; a 1 cm^2 platinum foil was used as counter electrode. All potentials are reported *vs.* SCE. Electrochemical impedance spectroscopy measurements (EIS) were performed using a Gamry instrument Potentiostat/Galvanostat with a Gamry framework system based on ESA 400 in a frequency range of 100,000 Hz to 0.01 Hz under potentiodynamic conditions, with amplitude of 10 mV peak-to-peak, using AC signal at E_{corr}. Gamry applications include software DC105 for corrosion and EIS300 for EIS measurements, and Echem Analyst version 5.50 software packages for data fitting. The experiments were measured after 30 min. of immersion in the testing solution (no deaeration, no stirring).

The inhibition efficiency of the inhibitor was calculated from the charge transfer resistance values using the following Eqn:

$$\mu_{R_{ct}}\% = \frac{R_{ct}^{i} - R_{ct}^{0}}{R_{ct}^{i}} \times 100 \quad (1)$$

where R_{ct}^{0} and R_{ct}^{i} are the charge transfer resistance in absence and in presence of inhibitor, respectively.

2.4 Potentiodynamic polarization

The electrochemical behaviour of mild steel sample in inhibited and non-inhibited solution was studied by recording anodic and cathodic potentiodynamic polarization curves. Measurements were performed in the 1 M HCl solution containing different concentrations of the tested inhibitor by changing the electrode potential automatically from -250 to +250 mV *vs.* corrosion potential at a scan rate of 1 mV s^{-1}. The linear Tafel segments of anodic and cathodic curves were extrapolated to corrosion potential to obtain corrosion current densities (i_{corr}).

The inhibition efficiency was evaluated from the measured i_{corr} values using the relationship:

$$\mu_{\mathrm{p}}\% = \frac{i_{\mathrm{corr}}^{0} - i_{\mathrm{corr}}^{\mathrm{i}}}{i_{\mathrm{corr}}^{0}} \times 100 \quad (2)$$

where, i_{corr}^{0} and $i_{\mathrm{corr}}^{\mathrm{i}}$ are the corrosion current density in absence and presence of inhibitor, respectively.

2.5 Linear polarization measurement

The corrosion behaviour was studied with polarization resistance measurements (R_{p}) in 1 M HCl solution with and without different concentrations of studied inhibitor. The linear polarization study was carried out from cathodic potential of -20 mV *vs.* OCP to an anodic potential of + 20 mV *vs.* OCP at a scan rate 0.125 mV s^{-1} to study the polarization resistance ($R_{\mathrm{p})}$ and the polarization resistance was evaluated from the slope of curve in the vicinity of corrosion potential. From the evaluated polarization resistance value, the inhibition efficiency was calculated using the relationship:

$$\mu_{R_{\mathrm{p}}}\% = \frac{R_{\mathrm{p}}^{\mathrm{i}} - R_{\mathrm{p}}^{0}}{R_{\mathrm{p}}^{\mathrm{i}}} \times 100 \quad (3)$$

where, R_{p}^{0} and $R_{\mathrm{p}}^{\mathrm{i}}$ are the polarization resistance in absence and presence of inhibitor, respectively.

2.6 Weight loss measurements

Weight loss measurements were performed on rectangular mild steel samples having size 2.5 × 2.0 × 0.025 cm by immersing the mild steel coupons into acid solution (100 mL) in absence and presence of different concentrations of CFM. After the elapsed time, the specimen were taken out, washed, dried and weighed accurately. All the tests were conducted in aerated 1 M HCl. All the experiments were performed in triplicate and average values were reported. From the evaluated corrosion rate, the surface coverage (θ) and inhibition efficiency ($\mu_{\mathrm{WL}}\%$) was calculated using:

$$\theta = \frac{C_{\mathrm{R}}^{0} - C_{\mathrm{R}}^{\mathrm{i}}}{C_{\mathrm{R}}^{0}} \quad (4)$$

$$\mu_{\mathrm{WL}}\% = \theta \times 100 \quad (5)$$

where, θ is surface coverage, C_{R}^{0} is corrosion rate in free acid solution and $C_{\mathrm{R}}^{\mathrm{i}}$ is corrosion rate in acid solution in presence of inhibitor, respectively.

3. RESULTS AND DISCUSSION

3.1 Electrochemical impedance spectroscopy

Impedance method provides information about the kinetics of the electrode processes and simultaneously about the surface properties of the investigated systems. The shape of impedance gives mechanistic information.

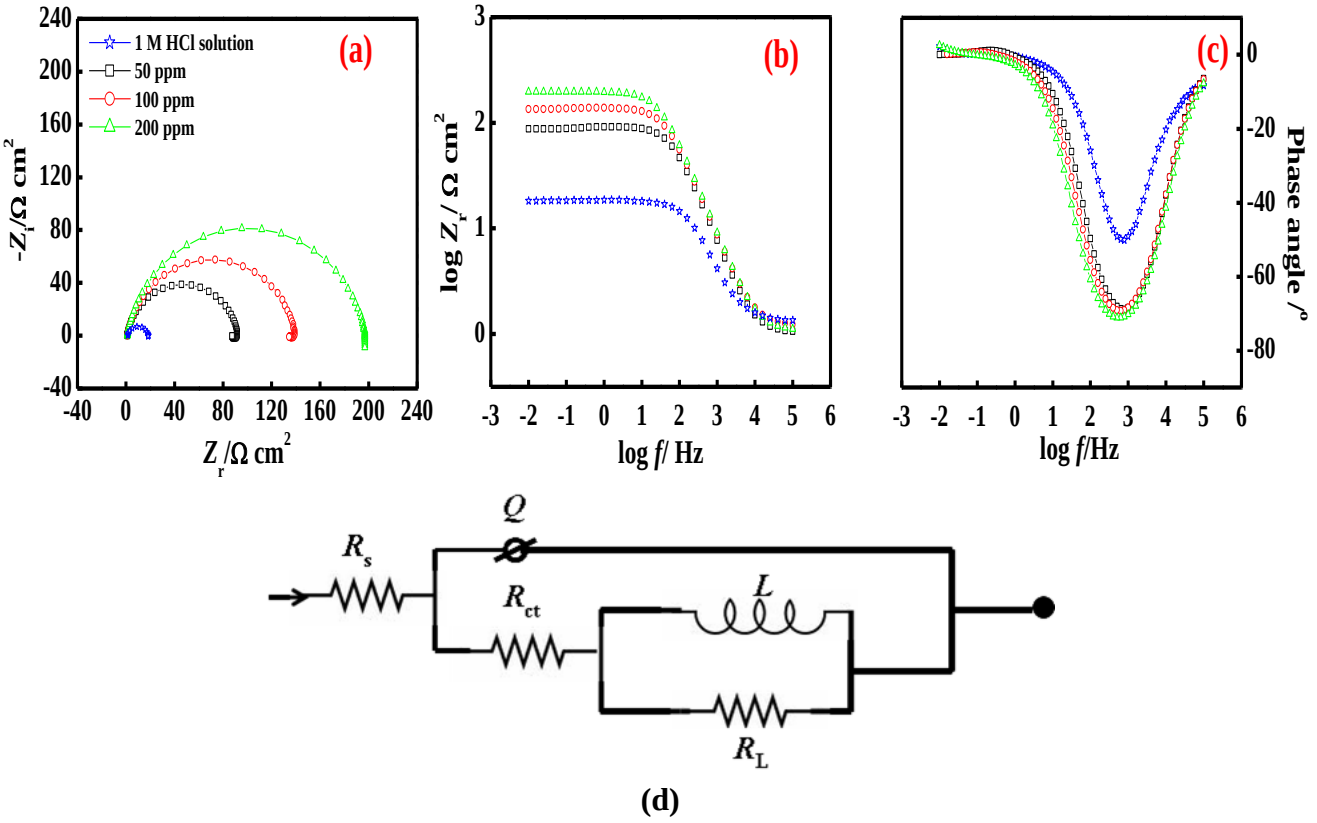

Figure 2. (a) Nyquist plot, (b) Bode-magnitude plot and (c) Phase angle plots obtained for the mild steel in 1 M HCl in the absence and presence of CFM and (d) The electrochemical equivalent circuit used to fit the impedance

The method is widely used for investigation of the corrosion inhibition processes [11]. Nyquist and Bode plots of mild steel in 1 M HCl solution in absence and presence of different concentrations of CFM are presented in Fig. 2a and 2b. It follows from Fig. 2a that a high frequency (HF) depressed charge-transfer semicircle was observed (one time constant in Bode plot) followed by a well defined inductive loop in the low frequency (LF) regions. The HF semicircle is attributed to the time constant of charge transfer and double-layer capacitance [12, 13]. The LF inductive loop may be attributed to the relaxation process obtained by adsorption species as Cl^-_{ads} and H^+_{ads} on the electrode surface [14].

Phase angle at high frequencies provided a general idea of anticorrosion performance. The more negative the phase angle the more capacitive the electrochemical behaviour [15]. Charge transfer

resistance increment could raise current tendency to pass through the capacitor in the circuit. Also, depression of phase angle at relaxation frequency with decreasing CFM concentration (Fig. 2c) indicated decrease of capacitive response with the decrease of inhibitor concentration. Such a phenomenon could be attributed to higher corrosion activity at low concentrations of inhibitor.

To get more accurate fit of these experimental data, the measured impedance data were analysed by fitting in to equivalent circuit given in Fig. 2d. The equivalent circuit consists of the double-layer capacitance (C_{dl}) in parallel to the charge transfer resistance (R_{ct}), which is in series to the parallel of inductive elements (L) and R_L. The presence of L in the impedance spectra in the presence of the inhibitor indicates that mild steel is still dissolved by the direct charge transfer at the CFM-adsorbed mild steel surface [3].

One constant phase element (CPE) is substituted for the capacitive element to give a more accurate fit, as the obtained capacitive loop is a depressed semi-circle. The depression in Nyquist semicircles is a feature for solid electrodes and often referred to as frequency dispersion and attributed to the roughness and other inhomogenities of the solid electrode [16]. The CPE is a special element whose admittance value is a function of the angular frequency (ω), and whose phase is independent of the frequency. The admittance and impedance of CPE is given by;

$$Y_{CPE} = Y_0(i\omega)^n \qquad (6)$$

where, Y_0 is the magnitude of CPE, i is an imaginary number ($i^2 = -1$) α is the phase angle of CPE and $n = \alpha/(\pi/2)$ in which α is the phase angle of CPE.

Table 1. Impedance parameters for mild steel in 1 M HCl in absence and presence of different concentrations of CFM

Inhibitor	Conc. (ppm)	R_s (Ω cm^2)	Q ($10^{-6} \times \Omega^{-1}$ s^n cm^{-2})	n	L (H)	R_{ct} (Ω cm^2)	R_L (Ω cm^2)	$\mu_{R_{ct}}$ %
CFM	-	1.30	164.0	0.811	13.0	16.0	1.0	-
	50	1.03	52.9	0.847	2.6	86.5	4.9	81.5
	100	1.20	51.9	0.883	5.5	133.9	4.7	88.0
	200	0.91	41.8	0.898	35.9	194.3	3.4	91.8

The point of intersection between the inductive loop and the real axis represents ($R_s + R_{ct}$). The electrochemical parameters, Including R_s, R_{ct}, R_L, L, Y_0 and n, obtained from fitting the recorded EIS using the electrochemical circuit of Fig. 2d are listed in Table 1. C_{dl} values derived from CPE parameters according to equation (7) are listed in Table 1.

$$C_{dl} = Y_0(\omega_{max})^{n-1} \qquad (7)$$

where, ω_{max} is angular frequency ($\omega_{max} = 2\pi f_{max}$) at which the imaginary part of impedance ($-Z_i$) is maximal and f_{max} is AC frequency at maximum.

3.2 Potentiodynamic polarization measurements

Polarization measurements were carried out in order to gain knowledge concerning the kinetics of the cathodic and anodic reactions. Fig.3 shows the results of the effect of CFM concentration on the cathodic and anodic polarization curves of mild steel in 1 M HCl, respectively. It could be observed that both the cathodic and anodic reactions were suppressed with the addition of CFM, which suggested that the CFM reduced anodic dissolution and also retarded the hydrogen evolution reaction.

Electrochemical corrosion kinetics parameters, i.e. corrosion potential (E_{corr}), cathodic and anodic Tafel slopes (b_a, b_c) and corrosion current density (i_{corr}) obtained from the extrapolation of the polarization curves, were given in Table 2.

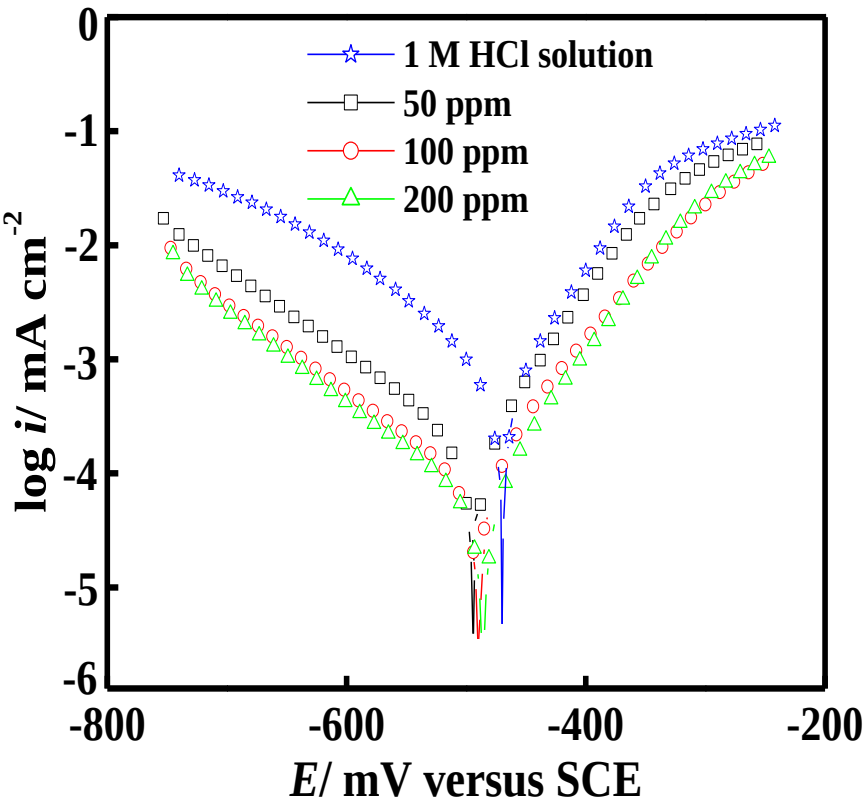

Figure 3. Typical polarization curves for corrosion of mild steel in 1 M HCl in the absence and presence of different concentrations of CFM

Fig. 3 represents the potentiodynamic polarization curves of mild steel in 1M HCl in the absence and presence of various concentrations of the CFM. It can be seen from the Fig. 3 that, in the presence of inhibitor, the curves are shifted to lower current regions, showing the inhibition tendency of the CFM. There was no definite trend is observed in the E_{corr} values in the presence of CFM. In the present study, shift in E_{corr} values is in the range of 20-25 mV suggested that they all are acted as mixed type of inhibitor [4, 17]. The values of various electrochemical parameters derived by Tafel polarization of all the inhibitors are given in Table 2.

Table 2. Potentiodynamic polarization parameters for mild steel without and with different concentrations of CFM in 1 M HCl

Inhibitor conc. (ppm)	Tafel data					Linear polarization data	
	$-E_{corr}$ (mV *vs.* SCE)	i_{corr} (μA cm^{-2})	b_a (mV dec^{-1})	$-b_c$ (mV dec^{-1})	μ_P%	R_p (Ω cm^2)	μ_{R_p} %
-	469	730	73	127	-	19	-
50	494	138	72	128	81.1	97	80.4
100	490	102	73	193	86.0	144	86.8
200	486	76	70	185	89.6	288	93.4

Investigation of Table 2 revealed that the values of b_a change slightly in the presence of CFM where as more pronounced change occurs in the values of b_c, indicating that both anodic and cathodic reactions are effected but the effect on the cathodic reactions is more prominent. Thus, CFM acted as mixed type, but predominantly cathodic inhibitor [18]. Increase in inhibition efficiencies with increasing concentration of CFM reveals that inhibition action is due to adsorption on steel surface and the adsorption is known to depend on the chemical structure of the inhibitors.

3.3 Linear polarization resistance

Polarization resistance values were determined from the slope of the potential-current lines,

$$R_p = A\frac{dE}{di} \quad (8)$$

Where, A is the surface area of electrode, dE is change in potential and di is change in current. The inhibition efficiencies and polarization resistance parameters are presented in Table 2. The results obtained from Tafel polarization and EIS showed good agreement with the results obtained from linear polarization resistance.

3.4 Weight loss measurements

3.4.1 Effect of inhibitor concentration

The variation of inhibition efficiency (μ_{WL}%) with inhibitor concentration is shown in Fig.4a. Better inhibition efficiency at higher concentration may be attributed to larger coverage of metal with inhibitor molecules.

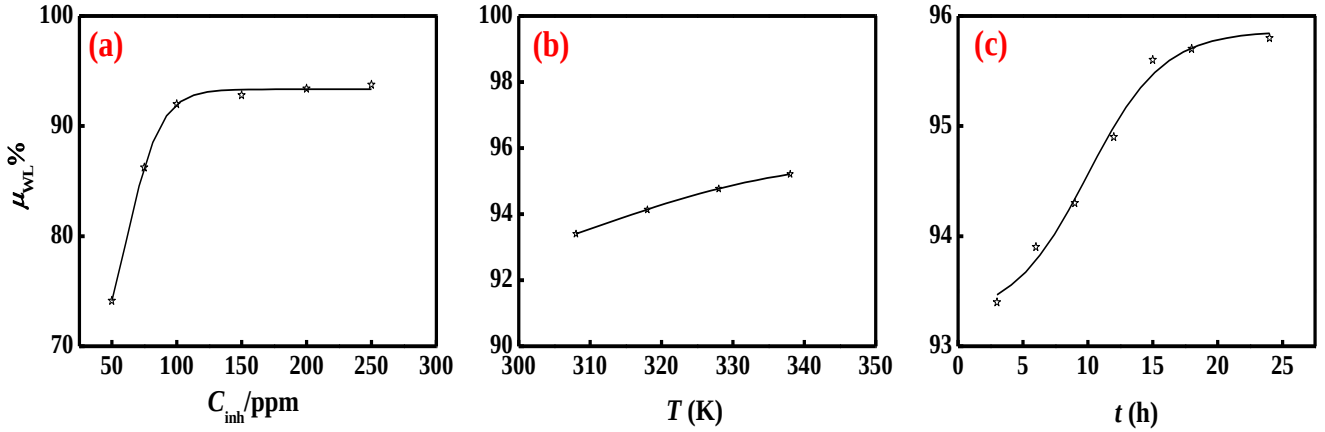

Figure 4. Variation of inhibition efficiency of CFM with (a) inhibitor concentration, (b) temperature of solution and (c) immersion time

3.4.2 Effect of temperature

The values of inhibition efficiencies obtained from weight loss measurement for the optimum concentration of CFM (200 ppm) in 1 M HCl are shown in Fig. 4b. From Fig. 4b, it can be seen that inhibition efficiency slightly increased with increasing temperature. This behaviour led to the conclusion that a protective film of CFM formed on the mild steel surface is thermally stable up to 338 K.

3.4.3 Effect of immersion time

Fig. 4c shows the effect of immersion time (3-24 h) at 308 K on the inhibition efficiency of CFM at 200 ppm concentration. Fig. 4c showed that CFM inhibits the corrosion of mild steel for all immersion times. The inhibition efficiency of CFM increased first from 3 to 15 h and thereafter almost constant suggesting the formation of persistent film on the metal surface.

3.4.4 Thermodynamic activation parameters

The dependence of corrosion rate on temperature can be expressed by Arrhenius equation and transition state equation [19, 20]:

$$\log(C_R) = \frac{-E_a}{2.303RT} + \log\lambda \quad (9)$$

$$C_R = \frac{RT}{Nh}\exp\left(\frac{\Delta S^*}{R}\right)\exp\left(-\frac{\Delta H^*}{RT}\right) \quad (10)$$

where E_a is the apparent activation energy, λ the pre-exponential factor, ΔH^* the apparent enthalpy of activation, ΔS^* the apparent entropy of activation, h Planck's constant and N the Avogadro number, respectively.

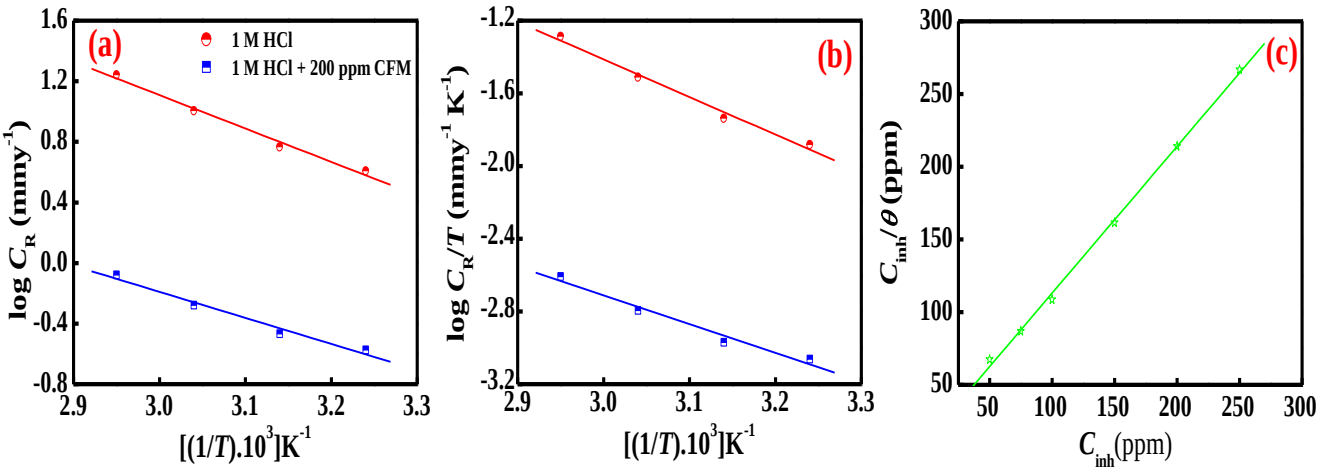

Figure 5. (a) Arrhenius plot of log *C*R versus 1/*T* and (b) log (*C*R/*T*) versus 1/*T* in absence and presence of 200 ppm CFM and (c) Langmuir adsorption isotherm.

The apparent activation energy and pre-exponential factors at 200 ppm concentration of CFM can be calculated by linear regression between $\log C_R$ and $1/T$ and the results are presented in Table 3. All the linear regression coefficients are close to 1, indicating that corrosion of mild steel in hydrochloric acid can be explained using the kinetic model.

Table 3. Thermodynamic parameters of activation for mild steel in 1 M HCl in absence and presence of different concentrations of CFM.

Inhibitor Conc. (ppm)	E_a (kJ mol^{-1})	λ (mmy^{-1})	ΔH^* (kJ mol^{-1})	ΔS^* (J mol^{-1} K)
-	42.21	5.31× 10^8	39.55	-86.75
200	32.90	9.30× 10^4	30.25	-129.97

Fig. 5a depicts an Arrhenius plot for mild steel immersed in 1 M HCl in absence and presence of 200 ppm CFM. The plots obtained are straight lines and the slope of each straight line gives its apparent activation energy. Table 3 summarizes E_a value for a 200 ppm CFM. Inspection of Table 3 showed that apparent activation energy decreased in the presence of CFM. The decrease in activation energy may be interpreted as chemisorption [21]. According to equation [9], corrosion rate (C_R) is being affected by both E_a and λ. In general, the influence of E_a on the mild steel corrosion was higher than that of λ on the mild steel corrosion. However, if the variation in λ was drastically higher than that of E_a, the value of λ might be the dominant factor to determine the mild steel corrosion. In the present

case, E_a and λ decreased in the presence of inhibitor (the higher E_a and lower λ led to lower corrosion rate). Hence, it is clear that lowering of λ is the decisive factor affecting the corrosion rate of mild steel in 1 M HCl.

The relationship between $\log(C_R/T)$ and $1/T$ is shown in Fig. 5b. The value of ΔH^* and ΔS^* were calculated and presented in Table 3. The positive sign of enthalpy reflect the endothermic nature of steel dissolution process meaning that dissolution of steel is difficult [22].

On comparing the values of the entropy of activation (ΔS^*) given in Table 3, it is clear that entropy of activation decreased in the presence of CFM than in the absence of inhibitor. The lowering of ΔS^* reveals that decrease in disordering takes place on going from reactant to the activated complex [23].

3.4.5 Adsorption isotherm

The adsorption on the corroding surfaces never reaches the real equilibrium and tends to reach an adsorption steady state. When corrosion rate is sufficiently decreased in the presence of inhibitor, the adsorption steady state has a tendency to attain quasi-equilibrium state. Now, it is reasonable to consider quasi-equilibrium adsorption in thermodynamic way using the appropriate adsorption isotherm. The degree of surface coverage (θ) for inhibitor was obtained from average weight loss data. Langmuir, Frumkin and Temkin adsorption isotherms were tested in order to find the best fit adsorption isotherm for adsorption of CFM on the surface of mild steel from 1 M HCl solution. Since, the linear regression coefficient of Langmuir adsorption isotherm is found more close to unity hence, was found best fit (Fig. 5c). With regard to the Langmuir adsorption isotherm the surface coverage (θ) of the inhibitor on the mild steel surface is related to the concentration (C_{inh}) of the inhibitor in the bulk of the solution according to the following equation:

$$\theta = \frac{K_{ads} C_{inh}}{1 + K_{ads} C_{inh}} \tag{11}$$

where, K_{ads} is the equilibrium constant for the adsorption/desorption process. This equation can be rearranged to

$$\frac{C_{inh}}{\theta} = \frac{1}{K_{ads}} + C_{inh} \tag{12}$$

It is a known fact that K_{ads} represents the strength between adsorbate and adsorbent. Large values of K_{ads} imply more efficient adsorption and hence better inhibition efficiency [24].

From the intercepts of the straight lines on the C_{inh}/θ-axis (Fig. 5c), K_{ads} can be calculated which is related to free energy of adsorption, ΔG^o_{ads} as given by Eqn. 13.

$$\Delta G^o_{ads} = -RT \ln(55.5 K_{ads}) \tag{13}$$

The calculated values of K_{ads}, ΔG^{o}_{ads} and linear regression coefficient R^2 are presented in Table 4. The negative values of ΔG^{o}_{ads} ensure the spontaneity of the adsorption process and stability of the adsorbed film on the mild steel surface [25, 26].

Table 4. Calculated parameters for Langmuir adsorption isotherm

Temperature (K)	K_{ads} (M^{-1})	$-\Delta G^{o}_{ads}$ (kJ mol^{-1})
308	3.0×10^4	36.7
318	3.4×10^4	38.2
328	3.8×10^4	39.7
338	4.2×10^4	41.2

4. MECHANISM OF INHIBITION

From the results obtained from the electrochemical and weight loss measurements, it was concluded that CFM inhibit the corrosion of mid steel in 1 M HCl by adsorption at mild steel/solution interface. It is a general assumption that the adsorption of organic inhibitors at the metal surface interface is the first step in the mechanism of the inhibitor action. Organic molecules maybe adsorbed on the metal surface in four ways namely;

(i) electrostatic interaction between the charged molecules and the charged metal,

(ii) interaction of unshared electron pairs in the molecule with the metal,

(iii) interaction of π-electrons with the metal and

(iv) a combination of types (i-iii) [6, 27-28]

The structure of CFM contains non-bonded electrons of hetero-atoms, free amino group as well as π-electron clouds of aromatic ring. In the aqueous HCl solution, CFM exists either as neutral molecule or as cation. In the aqueous HCl solution, CFM may be adsorbed on the surface of mild steel in the form of neutral molecule by replacing water molecules. CFM molecules are also adsorbed through electrostatic interactions between positively charged nitrogen atoms and negatively charged mild steel surface. Further, CFM molecules are chemically adsorbed due to interaction of π- orbitals with metal surface following deprotonation step of the physically adsorbed protonated molecules.

5. CONCLUSION

The following main conclusions are drawn from the present study:

1. CFM was found to be a good inhibitor for mild steel corrosion in acid medium.

2. The increasing values of "n" indicated the decreasing roughness of mild steel surface with CFM concentration.

3. The negative values of ΔG^{o}_{ads} indicated that the adsorption of the inhibitor molecule is a spontaneous process and an adsorption mechanism is typical of chemisorption.

4. Potentiodynamic polarization curves revealed that CFM is a mixed-type predominantly cathodic inhibitor.

5. The adsorption of CFM obeyed Langmuir adsorption isotherm.

ACKNOWLEDGEMENT
One of the authors A. K. S. is thankful to University Grant Commission (UGC), New Delhi, for Senior Research Fellowship and the North West University (South Africa) for a Postdoctoral Fellowship.

References

1. G. Trabanelli, *Corrosion* 47 (1991) 410.
2. D. D. N. Singh, T. B. Singh, B. Gaur, *Corros. Sci*.37 (1995) 1005.
3. A.K. Singh, M. A. Quraishi, *J. Appl. Electrochem.* 40 (2010) 1293.
4. A.K. Singh, M. A. Quraishi, *Corros. Sci.* 52 (2010) 1529.
5. E. E. Oguzie, B. N. Okolue, E. E. Ebenso, G. N. Onuoha, A. I. Onuchukwu, *Mater. Chem. Phys.* 87 (2004) 394.
6. A.K. Singh, M. A. Quraishi, *Corros. Sci.* 52 (2010) 152
7. O. K. Abiola, A.O. James, *Corros. Sci.* 52 (2010) 661.
8. A.K. Singh, M. A. Quraishi, *J. Appl. Electrochem.* 41 (2011) 7.
9. E. S. Ferreira, C. Giacomelli, F. C. Giacomelli, A. Spinelli, *Mater.Chem. Phys.* 83 (2004) 129
10. S. K. Shukla, A. K. Singh, I. Ahamad, M. A. Quraishi, *Mater. Lett.* 63 (2009) 819
11. A.K. Singh, M. A. Quraishi, *Mater. Chem. Phys.* 123 (2010) 666.
12. C. Deslouis, B. Tribollet, G. Mengoli, M. M. Musiani, *J. Appl. Electrochem.* 18 (1988) 374.
13. S. S. Abdel Rehim, H. H. Hassan, M. A. Amin, *Appl. Surf. Sci.*, 187 (2002) 279.
14. A.K. Singh, M. A. Quraishi, *Corros. Sci.* 52 (2010) 1373.
15. S.O. Niass, M. Ebn Touham, N. Hajjaji, A. Srhiri, H. Takenouti, *J. Appl. Electrochem.* 31 (2001) 85.
16. M. Mahadavian, M. M. Attar, *Corros. Sci.* 48 (2006) 4152.
17. O. L. Riggs Jr., Corrosion Inhibitors, 2nd ed., (1973) C.C. Nathan, Houston, TX
18. K. F. Khaled, N. Hackerman, *Electrochim. Acta* 48 (2003) 2715
19. X. Li, L. Tang, *Mater. Chem. Phys.* 90 (2005) 286
20. E. A. Noor, A. H. Al-Moubaraki, *Mater. Chem. Phys.* 110 (2008) 145
21. E.F. El Sherbini, *Mater. Chem. Phys.* 60 (1999) 286.
22. N.M. Guan, L. Xueming, L. Fei, *Mater. Chem. Phys.* 86 (2004) 59
23. E. Khamis, A. Hosney, S. El-Khodary, *Afinidad* 52 (1995) 95
24. L. Tang, X. Li, Y. Si, G. Mu, G.H. Liu, *Mater. Chem. Phys.* 95 (2006) 26
25. H. Keles, M. Keles¸ I. Dehri, O. Serindag, *Colloids and Surfaces A: Physicochem. Eng. Aspects* 320 (2008) 138.
26. A.K. Singh, M.A. Quraishi, *Corros. Sci.* 51 (2009) 2752
27. D.P. Schweinsberg, G.A. George, A.K. Nanayakkara, D.A. Steiner, *Corros. Sci.* 28 (1988) 33.
28. H. Shorky, M. Yuasa, I. Sekine, R.M. Issa, H.Y. El-Baradie, G.K. Gomma, *Corros. Sci.* 40 (1998) 2173.

© 2011 by ESG (www.electrochemsci.org)